

Article

Buckling Analysis of a Composite Honeycomb Reinforced Sandwich Embedded with Viscoelastic Damping Material

Dezhong Qi ¹, Qiang Sun ¹, Sanqiang Zhang ¹, Yuanfang Wang ^{2,*} and Xiaoqiang Zhou ³

¹ Hubei Agricultural Machinery Engineering Research and Design Institute, Hubei University of Technology, Wuhan 430068, China

² Railway Locomotive and Vehicle Institute, Wuhan Railway Vocational College of Technology, Wuhan 430205, China

³ Department of Mechanics, School of Aerospace Engineering, Huazhong University of Science and Technology, Wuhan 430074, China

* Correspondence: yuanfangwang@wru.edu.cn

Abstract: In this study, the buckling loads of a composite sandwich structure, which is reinforced by a honeycomb layer and filled with viscoelastic damping material, are analyzed. By applying von Karman anisotropic plate equations for large deflection, the governing equation of the composite sandwich structure is determined, and the deflection of the structure is further defined by a double triangular series. According to the dynamic equivalent effective stiffness obtained by the homogenous asymptotic method and Hill's generalized self-consistent model based on the Halpin–Tsai model, limiting the dynamic load buckling of the composite honeycomb reinforced sandwich structure embedded with viscoelastic damping material under axial compression can be achieved. The factors that influence the composite sandwich's buckling loads are discussed and compared, such as the load and geometry parameters, the thickness of the honeycomb reinforcement layer and the honeycomb's width. Finally, the results obtained by the present method are validated by the existing literature.

Keywords: buckling; viscoelastic damping material; honeycomb reinforcements; sandwich plate



Citation: Qi, D.; Sun, Q.; Zhang, S.; Wang, Y.; Zhou, X. Buckling Analysis of a Composite Honeycomb Reinforced Sandwich Embedded with Viscoelastic Damping Material. *Appl. Sci.* **2022**, *12*, 10366. <https://doi.org/10.3390/app122010366>

Academic Editors: Stelios K. Georgantzinos, Stylianos Markolefas, Georgios I. Giannopoulos and Konstantinos Stamoulis

Received: 14 September 2022

Accepted: 11 October 2022

Published: 14 October 2022

Publisher's Note: MDPI stays neutral with regard to jurisdictional claims in published maps and institutional affiliations.



Copyright: © 2022 by the authors. Licensee MDPI, Basel, Switzerland. This article is an open access article distributed under the terms and conditions of the Creative Commons Attribution (CC BY) license (<https://creativecommons.org/licenses/by/4.0/>).

1. Introduction

In engineering applications, structure stability evaluation is more important than stiffness and strength in most cases. On most occasions, structures fail due to instability factors, such as the structure's buckling, and as is known, the critical buckling loads of the structure are far smaller than the allowable loads. Quebec bridge disasters are usually considered as buckling failures and instability problems, as is known in engineering [1]. Today, to achieve high stiffness/hardness, considerable toughening, light-weight properties and composite materials and structures are introduced into engineering applications, which have been capturing more and more researchers' attention. Therefore, the buckling analysis of the composite structures is performed extensively in many different fields of engineering, such as aviation, navigation and mechanical engineering [2]. Accordingly, the buckling characteristics are taken into consideration. As pointed out by Wang et al. [3], the buckling of the structure is an important consideration in structural design, especially when the structure is slender and lightweight. Sayyad and Ghugal [4] presented a state-of-the-art discussion and critical review on the bending and buckling analysis of composite laminated structures, especially on comparisons of the methodologies and discussion of the composite structures, such as laminate theories and numerical methods. By applying the numerical and experimental methods, Namdar and Darendeliler [5] examined the buckling and failure process of a composite laminated structure made by bi-directional and oven fabric laminae. By employing the Kelvin–Voigt model and basing their work on nonlocal elastic theory, Kolehchi et al. [6] developed the refined Zigzag theory to analyze the dynamic buckling of laminated nano-plates. The factors that influence the structure's dynamic buckling were

thoroughly explored, such as the viscoelastic layer's damping coefficient, aspect ratio, various boundary conditions, etc. Based on the cell-based smoothed discrete shear gap method mixed-variable differential evolution theory, Ho-Huu et al. [7] proposed a novel numerical optimization procedure with mixed-integer and continuous design variables for the optimal design of laminated composite plates' buckling loads. To maximally increase the buckling loads of the composite laminated plate, thin composite grid layers were proposed by Ehsani and Rezapazhand [8] by combining the first-order shear deformation and classical laminated plate theories, and a genetic algorithm was utilized to optimize the stacking sequence and pattern composition of grid composite laminate. In the present analysis, as a type of grid, the honeycomb reinforced layer is applied and embedded in the laminated structure. The buckling response characteristic of the grid stiffened laminated composite plates was also analyzed by Huang et al. [9] by the finite element model. By introducing a unique Fourier series function to describe the longitudinal variation of deflection, Chen and Qiao [10] developed a novel semi-analytical finite strip method to predict the buckling properties of the composite laminated structures. Based on the first-order shear deformation theory and a combination of the modified couple stress theory, Arshid et al. [11] analyzed the bending and buckling characteristics of a heterogeneous annular/circular micro sandwich plate located on the Pasternak foundation.

The critical buckling analysis of composite laminated structures is focused on static changes in external loads, which are either very tiny or neglected. However, in mechanical engineering, the external loads and working environments are changeable. Moreover, after the composite material is introduced in engineering, the dynamic characteristic of the materials should be considered for perusing a higher analysis result. Therefore, the dynamic critical buckling properties of the composite structure are required to consider. By considering the honeycomb structure applied and analyzed in engineering structures, such as honeycomb reinforced laminated beams [12–15], plates [16–24] and shells [25–27], to enhance the structure's stiffness or to strengthen it, the honeycomb reinforced layer is introduced in the present analysis. Through a stress function approach, Southward et al. [13] analyzed the buckling response of a composite laminated beam with a honeycomb core on a Winkler foundation. Through a two-scale theory of the updated Lagrangian type, Ohno et al. [17] analyzed the buckling of elastic square honeycomb structures subject to in-plane biaxial compression, and the results were validated by the energy method. Qiu et al. [16] examined the buckling of honeycomb structures under out-of-plane loads. Three types of honeycomb were considered, and finally, the results were validated by numerical and experimental methods. By applying the asymptotic homogenous method and basing their work on laminated plate theory, Zhou et al. [23] examined the dynamic equivalent effective modulus of the composite laminated structures with a honeycomb reinforced core, and factors that affect the structure's dynamic modulus were qualitatively and quantitatively discussed and compared.

Compared to the buckling analysis of the traditional analysis, the external energy applied to the laminated structure is transformed into strain energy and potential energy, and the energies are stored or transformed in the structure, which do not dissipate. Consequently, instability happens when the loads reach critical buckling, and finally, failure may occur. Moreover, the flows of material and tiny fractures of the composite structure may appear microscopically, which can also absorb and dissipate a large amount of mechanical energy. For improving the critical buckling loads of the laminated structures, viscoelastic materials are applied. Viscoelastic materials can transform and dissipate the mechanical energy and improve the friction coefficient of the laminated structure in microscopically [28–33]. Moreover, the structure's toughness is enhanced by the viscoelastic material's visco- and friction-characteristic and mechanical energy dissipation properties. Aiming towards energy dissipation and vibration control, Jung and Aref [34] proposed a combined polymer composite damping system, and the structure consists of a polymer honeycomb and a viscoelastic solid material. Considering that the constrained layer dampers are extensively applied for passive vibration damping in fields of engineering, a

novelty honeycomb structure filled with viscoelastic damping material was proposed by Aumjaud et al. [35], which can improve the modal loss factor of the composite laminated structure efficiently.

Following the structures constructed by Zhou et al. [23], in the present analysis, honeycomb structures and viscoelastic material are applied. The laminate's stiffness and hardness can be significantly enhanced by honeycomb reinforcement layers, and its toughening and energy dissipation characteristics are improved at the same time by the viscoelastic material. Considering that the dynamic effective equivalent stiffness of the honeycomb structure with viscoelastic material is strongly influenced by the external load's frequency, the structure's buckling loads are affected by frequency too. Consequently, the dynamic critical buckling loads of honeycomb reinforced laminated structures with viscoelastic material are examined here. Moreover, the geometry and external load factors that affect the dynamic buckling load of composite structures are researched and compared in detail.

2. Mathematical Modeling

A mathematical model of the honeycomb reinforced composite laminated plate with coupling in-plane forces N_x and N_y on the x - and the y -axis is shown in the following figures. The length and width of the composite laminate are denoted as a and b . The middle layer is composed of a honeycomb reinforcement structure and viscoelastic material fillers. The honeycomb structure is made of elastic material, and the fillers are viscoelastic material. The thickness of the three-layered composite laminated structure is illustrated in Figure 1c, and the laminated structure in the present analysis is considered as the symmetrical composite structure. The thickness of the two face layers is t_1 and t_3 , and the honeycomb reinforced layer is t_2 .

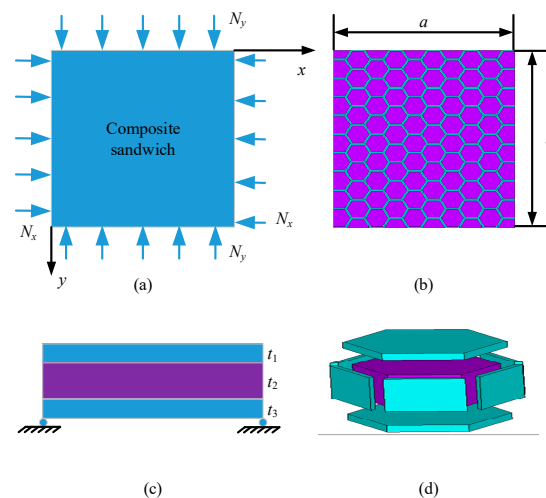


Figure 1. Buckling of the honeycomb reinforced laminated composite plate with two-direction forces. (a) Macroscopic of composite laminate sandwich; (b) Honeycomb reinforced composite core layer; (c) Boundary condition of the sandwich structure; (d) A representative unit cell of the sandwich.

3. Methodologies and Theoretical Derivation

In this analysis, the critical buckling load determination mainly contains two sections: the determination of the critical buckling equation and the prediction of the effective dynamic stiffness modulus of the composite sandwich. The determination of the critical buckling equation is performed based on large deflection theory, and the effective dynamic stiffness modulus of the composite sandwich is obtained through the homogenous asymptotic theory. More detail is presented in the following subsections.

3.1. Critical Buckling Equation Determination

According to von Karman’s anisotropic plate equations for large deflection [36,37], the governing equation of the composite sandwich structure under two directions of in-plane forces can be expressed as

$$D_{11} \frac{\partial^4 w}{\partial x^4} + 4D_{16} \frac{\partial^4 w}{\partial x^3 \partial y} + 2(D_{12} + 2D_{66}) \frac{\partial^4 w}{\partial x^2 \partial y^2} + 4D_{26} \frac{\partial^4 w}{\partial x \partial y^3} + D_{22} \frac{\partial^4 w}{\partial y^4} = N_x \frac{\partial^2 w}{\partial x^2} + 2N_{xy} \frac{\partial^2 w}{\partial x \partial y} + N_y \frac{\partial^2 w}{\partial y^2} - p_x \frac{\partial w}{\partial x} - p_y \frac{\partial w}{\partial y} - p_z \tag{1}$$

where w is the out-plane deflection of the composite anisotropic laminate, N_{xy} is the shear force, p_x , p_y and p_z are the distributed loads and D_{ij} is the bending stiffness. In the present analysis, the sandwich is considered a rectangle with four edges that are simply supported. Furthermore, we assume that there is an absence of shear and distributed loads, so the bending stiffness $D_{16} = D_{26} = 0$ can be considered. Moreover, only the axis loads are considered, and the shear forces on the laminated structure are not considered. Accordingly, the constitutive equation of the current problem can be obtained as

$$D_{11} \frac{\partial^4 w}{\partial x^4} + 2(D_{12} + 2D_{66}) \frac{\partial^4 w}{\partial x^2 \partial y^2} + D_{22} \frac{\partial^4 w}{\partial y^4} = N_x \frac{\partial^2 w}{\partial x^2} + N_y \frac{\partial^2 w}{\partial y^2} \tag{2}$$

For the simply supported rectangular plate, as shown in Figure 1c, the boundary conditions can be expressed as

$$w = M_x = -D_{11} \frac{\partial^2 w}{\partial x^2} - D_{12} \frac{\partial^4 w}{\partial y^4} = 0 \text{ at } x = 0, a \tag{3}$$

$$w = M_y = -D_{12} \frac{\partial^2 w}{\partial x^2} - D_{22} \frac{\partial^4 w}{\partial y^4} = 0 \text{ at } y = 0, b \tag{4}$$

To satisfy the boundary conditions as provided in the above equations, double sinusoidal series can be applied to express the deflection of the honeycomb reinforced composite laminated structure according to [38].

$$w = \sum_m^\infty \sum_n^\infty A_{mn} \sin \alpha x \sin \beta y \tag{5}$$

where A_{mn} denotes the amplitude of w , α and β are coefficients of the sinusoidal function and $\alpha = m\pi/a$, $\beta = n\pi/b$. By substituting Equations (3)–(5) into Equation (2), the following expression can be yielded:

$$\pi^2 A_{mn} [D_{11} m^4 + 2(D_{12} + 2D_{66}) m^2 n^2 \kappa_0 + D_{22} n^4 \kappa_a^4] = -A_{mn} a^2 [N_x m^2 + N_y n^2 \kappa_a^2] \tag{6}$$

When critical buckling appears on composite laminated structures, the in-plane deflection w is not zero. Accordingly, A_{mn} in the above equation can be deleted, and the buckling load of the honeycomb reinforced viscoelastic-material-composed sandwich structure can be achieved as

$$N_b = - \frac{\pi^2 [D_{11} m^4 + 2(D_{12} + 2D_{66}) m^2 n^2 \kappa_0 + D_{22} n^4 \kappa_a^4]}{a^2 (m^2 + k_n n^2 \kappa_a^2)} \tag{7}$$

where $k_n = N_x/N_y$, and the minus symbol in Equation (7) can be considered the compress force/load. We can find that the critical buckling load is independent of the amplitude of deflection, and it is correlated with the dynamical equivalent stiffness D_{ij} , the terms of the sinusoidal series m and n , the loading parameter k_n and the geometry parameter $\kappa_a = a/b$.

3.2. Equivalent Effective Modulus Determination

Considering that the laminated structures proposed in this analysis are periodically distributed in the x - y direction, as shown in Figure 1, and that a representative unit cell is shown according to the three-dimensional elastic theory [39], the elastic mechanics equilibrium equations of the laminated composites can be written as

$$\begin{cases} \sigma_{ij,j} = f_i \\ \sigma_{ij} = \frac{1}{2} C_{ijkl}(\alpha_1, \alpha_2, \gamma)(u_{k,l} + u_{l,k}) \\ \sigma_{ij} n_j^\pm = p_j^\pm \end{cases} \quad (8)$$

where $(\bullet)_{,j} = \partial(\bullet)_{,\alpha_j}$, C_{ijkl} is the fourth-order elasticity tensor of the material, f_i is the body force on the laminated structure, p_j^\pm represents the surface tractions on the top and bottom surfaces of the representative unit cell and $u_{l(k)}$ denotes displacements of the representative unit cell at the mid-plane in the $\alpha_{1(2)}$ direction. n_j^\pm is the normal vector of the representative unit cell's top and bottom surfaces and can be determined by $n^\pm = \frac{(\mp S^{\mp,\alpha_1}, \mp S^{\mp,\alpha_2}, 1)}{\sqrt{(S^{\mp,\alpha_1})^2 + (S^{\mp,\alpha_2})^2 + 1}}$.

3.3. Homogenous Asymptotic Methodologies

In this analysis, considering the periodic distribution of viscoelastic material and honeycomb reinforcements in geometry, the homogenous asymptotic theory is applied, and the "rapid" parameter ε is introduced. Asymptotic relationships can be written as

$$\xi_1 \rightarrow \frac{\alpha_1 A_1}{\varepsilon a}, \xi_2 \rightarrow \frac{\alpha_2 A_2}{\varepsilon b}, z \rightarrow \frac{\gamma}{(h_1 + h_2 + h_3)} \quad (9)$$

where a and b are the length and width of the sandwich laminate. The coordinate transformation through asymptotic theory can be expressed as

$$\begin{cases} \frac{\partial}{\partial \xi_1} \rightarrow \frac{\partial}{\partial \alpha_1} \frac{\partial \alpha_1}{\partial \xi_1} + \frac{\partial}{\partial \alpha_2} \frac{\partial \alpha_2}{\partial \xi_1} \\ \frac{\partial}{\partial \xi_2} \rightarrow \frac{\partial}{\partial \alpha_1} \frac{\partial \alpha_1}{\partial \xi_2} + \frac{\partial}{\partial \alpha_2} \frac{\partial \alpha_2}{\partial \xi_2} \end{cases} \quad (10)$$

Furthermore, the non-dimensional displacements of the representative volume element at the middle plane can be obtained according to the microscopic asymptotic theory

$$u_i(\alpha, \xi, z, \varepsilon) = u_i^{(0)}(\alpha) + \varepsilon u_i^{(1)}(\alpha, \xi, z) + \varepsilon^2 u_i^{(2)}(\alpha, \xi, z) + O(\varepsilon^3) \quad (11a)$$

$$\sigma_{ij}(\alpha, \xi, z, \varepsilon) = \varepsilon_{ij}^{(0)}(\alpha) + \varepsilon \sigma_{ij}^{(2)}(\alpha, \xi, z) + \varepsilon^2 \sigma_{ij}^{(2)}(\alpha, \xi, z) + O(\varepsilon^3) \quad (11b)$$

where $O(\varepsilon^3)$ means the infinitesimal of the higher-order term. The relationship between the displacements and stress tensors in the local coordinate for the representative volume element can be defined according to coordinate transform as

$$u_i = v_i(\alpha_1, \alpha_2) - \varepsilon \frac{z}{A_i} w(\alpha_1, \alpha_2)_{,\alpha_i} + \varepsilon U_i^{\mu\nu} \varepsilon_{\mu\nu} + \varepsilon^2 V_i^{\mu\nu} \tau_{\mu\nu} + O(\varepsilon^3) \quad (12a)$$

$$u_3 = w(\alpha_1, \alpha_2) + \varepsilon U_3^{\mu\nu} \varepsilon_{\mu\nu} + \varepsilon^2 V_3^{\mu\nu} \tau_{\mu\nu} + O(\varepsilon^3) \quad (12b)$$

$$\sigma_{ij} = b_{ij}^{\mu\nu} \varepsilon_{\mu\nu} + \varepsilon b_{ij}^{*\mu\nu} \tau_{\mu\nu} \quad (12c)$$

where $u_i(\alpha_1, \alpha_2)$, $v_i(\alpha_1, \alpha_2)$ and $w_i(\alpha_1, \alpha_2)$, respectively, represent the displacements in the α_i directions on the α_1 - α_2 plane. We can find from Equation (11a,b) that the general

global displacements and stresses of the representative volume element can be determined by the general local displacements $U_k^{\mu\nu}$ and $V_k^{*\mu\nu}$, where $U_k^{\mu\nu} = U_k^{\mu\nu}(\xi_1, \xi_2, z)$ and $V_k^{\mu\nu} = V_k^{\mu\nu}(\xi_1, \xi_2, z)$, and the local strain $\varepsilon_{\mu\nu}$ and $\tau_{\mu\nu}$ as well as $b_{ij}^{\mu\nu}$ and $b_{ij}^{*\mu\nu}$ denote the general local stress functions. $U_k^{\mu\nu}$ and $V_k^{*\mu\nu}$ can be obtained according to the physical behaviors of the viscoelastic material and elastic reinforcements, and they have three configurations, which can be expressed as

$$U_n^{\lambda\mu}(\xi_1, \xi_2, z) = \begin{cases} f(m_1\xi_1 + z) + g(m_2\xi_2 + z) & \Delta < 0 \\ f(m_1\xi_1 + z) + \xi_1 g(m_2\xi_2 + z) & \Delta = 0 \\ f(m_2\xi_2 + z) + g(m_1\xi_1 + z) & \Delta > 0 \end{cases} \quad (13a)$$

$$V_n^{\lambda\mu}(\xi_1, \xi_2, z) = \begin{cases} g(m_1\xi_1 + z) + f(m_2\xi_2 + z) & \Delta < 0 \\ g(m_1\xi_1 + z) + \xi_1 f(m_2\xi_2 + z) & \Delta = 0 \\ g(m_2\xi_2 + z) + f(m_1\xi_1 + z) & \Delta > 0 \end{cases} \quad (13b)$$

Applying the asymptotic expansion equations as shown in Equations (9) and (10), two intermediate functions with a double triangular style can be defined, which can be expressed as

$$f(\xi_1, \xi_2, z) = \begin{cases} \sum_{n=1}^N \sum_{m=1}^N \left[\sin\left(\frac{n\pi\xi_1}{\delta a} + z\right) \sin\left(\frac{m\pi\xi_1}{\delta b} + z\right) + \sin\left(\frac{n\pi\xi_1}{\delta b} + z\right) \sin\left(\frac{m\pi\xi_2}{\delta a} + z\right) \right] & \text{when } \Delta < 0 \\ \sum_{n=1}^N \sum_{m=1}^N \left[\sin\left(\frac{n\pi\xi_1}{\delta a} + z\right) \sin\left(\frac{m\pi\xi_1}{\delta b} + z\right) + \xi_1 \sin\left(\frac{n\pi\xi_1}{\delta b} + z\right) \sin\left(\frac{m\pi\xi_2}{\delta a} + z\right) \right] & \text{when } \Delta = 0 \\ \sum_{n=1}^N \sum_{m=1}^N \left[\sin\left(\frac{n\pi\xi_2}{\delta a} + z\right) \sin\left(\frac{m\pi\xi_2}{\delta b} + z\right) + \sin\left(\frac{n\pi\xi_1}{\delta b} + z\right) \sin\left(\frac{m\pi\xi_2}{\delta a} + z\right) \right] & \text{when } \Delta < 0 \end{cases} \quad (14a)$$

$$g(\xi_1, \xi_2, z) = \begin{cases} \sum_{n=1}^N \sum_{m=1}^N \left[\cos\left(\frac{n\pi\xi_2}{\delta a} + z\right) \cos\left(\frac{m\pi\xi_2}{\delta b} + z\right) + \cos\left(\frac{n\pi\xi_1}{\delta b} + z\right) \cos\left(\frac{m\pi\xi_1}{\delta a} + z\right) \right] & \text{when } \Delta > 0 \\ \sum_{n=1}^N \sum_{m=1}^N \left[\cos\left(\frac{n\pi\xi_2}{\delta a} + z\right) \cos\left(\frac{m\pi\xi_2}{\delta b} + z\right) + \xi_2 \cos\left(\frac{n\pi\xi_1}{\delta b} + z\right) \cos\left(\frac{m\pi\xi_1}{\delta a} + z\right) \right] & \text{when } \Delta = 0 \\ \sum_{n=1}^N \sum_{m=1}^N \left[\cos\left(\frac{n\pi\xi_1}{\delta a} + z\right) \cos\left(\frac{m\pi\xi_1}{\delta b} + z\right) + \cos\left(\frac{n\pi\xi_2}{\delta b} + z\right) \cos\left(\frac{m\pi\xi_2}{\delta a} + z\right) \right] & \text{when } \Delta > 0 \end{cases} \quad (14b)$$

The local deformations of each research object in two directions obtained by Equation (13) can be further written as $(U_k^{\mu\nu})^{(\Omega_n^{(L)})}$ and $(V_k^{*\mu\nu})^{(\Omega_n^{(L)})}$. Once they are determined, their general local stress tensors can be immediately evaluated, which can be written as $\langle E_{ij}^{\lambda\mu} \rangle^{(\Omega_n^{(L)})}$ and $\langle zE_{ij}^{*\lambda\mu} \rangle^{(\Omega_n^{(L)})}$. Then, the effective equivalent stiffness of the macroscopic composite sandwich structure in global coordinates can be achieved as follows:

$$\langle E_{ij}^{\lambda\mu} \rangle^{(G)} = \sum_{n=1}^N \langle E_{ij}^{\lambda\mu} \rangle^{(\Omega_n^{(L)})} \quad (15a)$$

$$\langle zE_{ij}^{*\lambda\mu} \rangle^{(G)} = \sum_{n=1}^N \langle zE_{ij}^{*\lambda\mu} \rangle^{(\Omega_n^{(L)})} \quad (15b)$$

where $\langle E_{ij}^{\lambda\mu} \rangle^{(G)}$ denotes the global effective modulus, and $\langle E_{ij}^{\lambda\mu} \rangle^{(\Omega_n^{(L)})}$ is the local effective modulus coefficient of the n th research object. In this analysis, a representative volume element consists of nine research objects. Therefore, $n = 9$ in Equation (16), and its local deformations, stresses and strains can be calculated individually. $\Omega_n^{(L)}$ means the analysis

object in the RVE of the composite structure. The superscripts in the brackets, L and G , denote the local coordinate and global coordinate, and these two systems are applied together to evaluate the global dynamic stiffness of the structure. In Equation (15), $ij\lambda\mu$ is the fourth-order elastic tensor of the viscoelastic/elastic material. In the present analysis, the fourth-order tensors of the materials are considered to be frequency dependent, and the viscoelastic/elastic materials are assumed to be isotropic. The Kelvin–Voigt single-subscript notation is applied, and this transformation can be written as [39].

$$\begin{aligned} (\bullet)_{11} &\rightarrow (\bullet)_1, (\bullet)_{22} \rightarrow (\bullet)_2 \\ (\bullet)_{33} &\rightarrow (\bullet)_3, (\bullet)_{23} \rightarrow (\bullet)_4 \\ (\bullet)_{13} &\rightarrow (\bullet)_5, (\bullet)_{12} \rightarrow (\bullet)_6 \end{aligned} \tag{16}$$

Finally, the dynamic equivalent effective stiffness of the honeycomb reinforced composite laminated structure can be determined as follows, according to [40]:

$$\langle \bullet(\xi_1, \xi_2, z) \rangle = \frac{1}{|V_\Omega|} \iiint_{V_\Omega} [\bullet(\xi_1, \xi_2, z)] d\xi_1 d\xi_2 dz \tag{17}$$

where $|V_\Omega|$ denotes the RVE’s volume. The mid-coefficient for the bending stiffness can be obtained as

$$\begin{cases} \bar{Q}_{ij} = \frac{\sum_{n=1}^N \langle E_{ij}^{\lambda\mu} \rangle^{(\Omega_n^{(L)})}}{1 - \langle v_{12}^{VR} \rangle \langle v_{21}^{VR} \rangle}, ij = 12, 21, 22 \\ \bar{Q}_{66} = \sum_{n=1}^N \langle z E_{ij}^{*\lambda\mu} \rangle^{(\Omega_n^{(L)})} \end{cases} \tag{18}$$

In Equation (18), $\langle v_{21}^{VR} \rangle$ is the equivalent dynamic Poisson’s ratio of the composite structure, and it can be approximately evaluated according to the composite laminated theory [41] as

$$\langle v_{12} \rangle = \left(t_1 + \frac{t_2}{2} \right) v_{12}^{VR} \langle E_{22}^{VR} \rangle / \left(t_1 E_{22}^R + \frac{t_2}{2} \langle E_{22}^{VR} \rangle \right) \tag{19}$$

where $\langle E_{22} \rangle$ is the equivalent modulus of the composite honeycomb reinforced layer, and it is composed of viscoelastic material and elastic material. The reinforcements are made of elastic material, and the filler is built of viscoelastic material. Then, it can be evaluated according to Hill’s generalized self-consistent model based on the Halpin–Tsai model [42–44] and macroscopically uniform theory [45]

$$E_{22}^{VR} = \frac{1}{\frac{f_R}{E_{22}^R} + \frac{f_{VEM}}{E_{22}^{VEM}} - f_{VEM} f_R \alpha_{tt}} \tag{20}$$

$$\alpha_{tt} = \frac{\frac{(v_R)^2 E_{22}^{VEM}}{E_{22}^R} + \frac{(v_{VEM})^2 E_{22}^R}{E_{22}^{VEM}} - 2v_R v_{VEM}}{f_R E_{22}^R + f_{VEM} E_{22}^{VEM}} \tag{21}$$

$$v_{12}^{VR} = f_R v_R + f_{VEM} v_{VEM} \tag{22a}$$

$$\rho^{VR} = f_R \rho_R + f_{VEM} \rho_{VEM} \tag{22b}$$

where f_{VEM} and f_R are the volume fractions of the viscoelastic material and the honeycomb reinforcement in a representative volume element, and v_R and v_{VEM} denote the Poisson’s ratio of reinforcements and viscoelastic fillers. The density of the honeycomb reinforced layer can be obtained through Equation (22a,b), and ρ_R and ρ_{VEM} denote the density of the viscoelastic and elastic materials.

By substituting the above equations into Equation (10), the dynamic equivalent Poisson’s ratio can be achieved. In the present analysis, the hexagonal honeycomb is considered; thus, $\langle v_{12} \rangle = \langle v_{21} \rangle$ can be assumed.

Accordingly, the dynamic equivalent bending stiffness of the honeycomb reinforced composite laminated with viscoelastic material can be obtained by drawing back the above equation into Equation (8) as

$$\langle D_{ij}^G \rangle = \begin{cases} \int_{-\frac{h}{2}}^{-\frac{h}{2}} \frac{\sum_{n=1}^N \langle E_{ij}^{\lambda\mu} \rangle^{(\Omega_n^{(L)})}}{1 - \langle v_{12}^{VR} \rangle \langle v_{21}^{VR} \rangle} z^2 dz, & ij = 12, 21, 22 \\ \int_{-\frac{h}{2}}^{-\frac{h}{2}} \sum_{n=1}^N \langle z E_{ij}^{*\lambda\mu} \rangle^{(\Omega_n^{(L)})} z^2 dz, & ij = 66 \end{cases} \quad (23)$$

Finally, the dynamic critical buckling loads of the composite honeycomb reinforced laminated can be determined as

$$\langle \widetilde{N}_b \rangle = - \frac{\pi^2 [\langle D_{11}^G \rangle m^4 + 2(\langle D_{12}^G \rangle + 2\langle D_{66}^G \rangle) m^2 n^2 k_a^2 + \langle D_{22}^G \rangle n^4 k_a^4]}{a^2(m^2 + k_n n^2 k_a^2)} \quad (24)$$

4. Numerical Analysis

In this section, a numerical analysis is performed. To visualize the regularity of the parameters’ influence on the critical buckling loads, the axis load parameter k_n , the geometry parameter k_a , the thickness ratio of the core layer, the honeycomb reinforcement’s width d_t and the dynamic impulse load’s frequency f are qualitatively and quantitatively compared and discussed. Geometrically, the external loads and physical parameters in the numerical section are defined as follows:

Geometrical parameters: face layers and honeycomb reinforcement.

$t_1 = 2.5$ mm, $t_2 = At_1$, $d_t = Bt_1$, where $A = \{2,4,8,12,16\}$, $B = \{1,2,3,4,5\}$.

$a = L_a = \{0.1:0.1:1\}$, $b = a/k_a$, $k_a = \{1:1:10\}$, $L_{\text{honey}} = a/10$. The fraction of the VEM filler and the hexagonal honeycomb reinforcement in the core layer are determined by L_{honey} and d_t .

Geometrical parameters: $N_y = k_n N_x = k_n N_0$, and $k_n = \{-2:0.5:2\}$. N_x and N_y denote the compression forces on the simply supported composite laminated structure, and the negative k_n means the tensile force.

Physical parameters: face layers and honeycomb reinforcement made of aluminum.

Poisson’s ratio $\nu_R = 0.33$, Young’s modulus $E_R = 68$ GPa, shear modulus $G_{R12} = 25.6$ Gpa, density $\rho_R = 2700$ kgm⁻³.

Physical parameters: VEM fillers.

Poisson’s ratio $\nu_{VEM} = 0.49$, density $\rho_{VEM} = 1200$ kgm⁻³. Young’s modulus and the shear modulus G_{R12} of the VEM are frequency dependent.

4.1. Critical Dynamic Buckling Load Affected by the Load Parameter k_n

As is known, the dynamic buckling of the composite structure is affected by two axial loads. The buckling load is changed if the tensional load is applied in one direction and if the compressional load is performed in the other direction. Moreover, the buckling load is variable when two compressional axial forces are loaded. To analyze the regularity and mechanism of the buckling loads affected by two axial forces, the load parameters of the honeycomb reinforced laminated composite structure are defined as k_n , where $N_y = N_0$ and $N_x = k_n N_y = k_n N_0$. The data are provided in Table 1. The buckling loads affected by k_n are plotted in Figure 2, where $k_a = 1$, and the length and width of the composite laminated plate are equal and denoted as a . $t_1 = t_3$, $t_2 = 4t_1$, $d_t = 1.5t_1$ and the length of the composite laminate ranges from 0.1 to 1 m. As shown in this figure, by increasing the load parameter, the buckling load is decreased significantly. Figure 3a shows that it is affected by the dimensions of the composite honeycomb reinforced laminate at the defined load

parameters, and the buckling loads are decreased by increasing the laminate’s geometry dimensions. To visualize the buckling load of the composite laminate quantitatively, the tensile and compression loads are numerically analyzed and plotted in Figure 3b. The reference load parameter is defined as $k_n = 1$, and the reference buckling load is N_0 ($k_n = 1$). The buckling load of the honeycomb reinforced laminate is increased by raising the tensile loads, whereas it is decreased by increasing the compression loads. It can be seen in the figure that the buckling load can be dramatically increased by the tensile forces, whereas it is decreased slowly by the compression forces.

4.2. Critical Buckling Load Affected by the Length/Width Geometry Parameter

Except for the dynamic equivalent effective stiffness of the honeycomb reinforced composite laminate, the critical dynamic buckling is directly influenced by the length and width of the honeycomb reinforced composite sandwich structure at the same time. The geometry shape of the composite structure is determined by the length–width ratio k_a . Accordingly, the critical dynamic buckling is affected by the geometrical parameter k_a . In this section, the critical dynamic buckling of the honeycomb reinforced laminated composite structure is analyzed numerically. In this section, $t_1 = t_3 = 2.5$ mm, $t_2 = 4t_1$, $d_t = 1.5t_1$, $k_n = 1$ and the buckling loads affected by k_a are shown in Table 2. The results are the same as those shown in Figure 4; the geometry dimensions of the composite laminate affect its buckling sharply by increasing the length and width of the composite structures, and the structure’s buckling is decreased significantly. However, it can be observed from Figure 5 that the structure’s buckling loads are increased by raising the geometry parameters, and a larger k_a can always provide a bigger one when the other parameters are defined. To analyze the rate changes in the buckling load on the geometrical parameters, Figure 6 is provided. It can be seen in this figure that the honeycomb reinforced composite structure’s buckling load sharply increases when k_a is smaller than five, but it slowly increases when k_a is larger than five in the considered ranges.

Table 1. Buckling loads vs. k_n .

a	0.1	0.2	0.3	0.4	0.5	0.6	0.7	0.8	0.9	1
$k_n = -2$	921.69	230.42	102.41	57.61	36.87	25.60	18.81	14.4	11.38	9.22
$k_n = -1.5$	582.62	145.66	64.74	36.41	23.30	16.18	11.89	9.10	7.19	5.83
$k_n = -1$	395.41	98.85	43.93	24.71	15.82	10.98	8.07	6.18	4.88	3.95
$k_n = 0$	307.70	76.93	34.19	19.23	12.31	8.55	6.28	4.81	3.80	3.08
$k_n = 1$	198.55	49.64	22.06	12.41	7.94	5.52	4.05	3.10	2.45	1.99
$k_n = 1.5$	153.49	38.37	17.05	9.59	6.14	4.26	3.13	2.40	1.89	1.53
$k_n = 2$	49.170	12.29	5.46	3.07	1.97	1.37	1.00	0.77	0.61	0.49

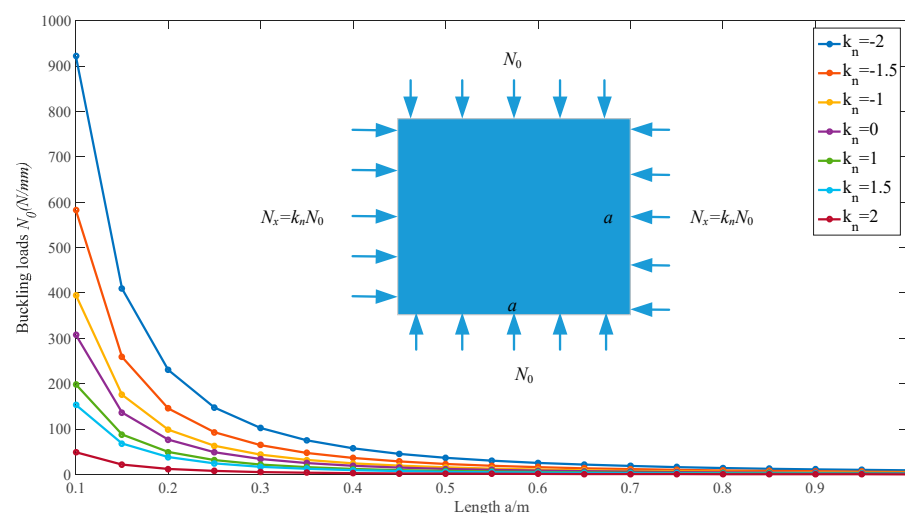


Figure 2. Buckling loads affected by axial force parameter.

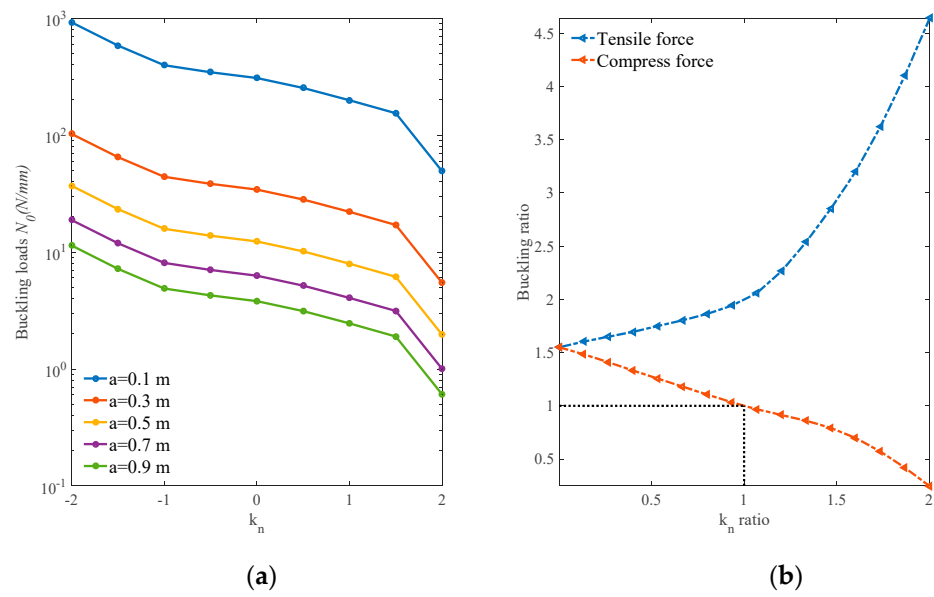


Figure 3. Buckling loads affected by axial force parameter. (a) k_n vs. Buckling loads, and (b) k_n ratio vs. Buckling load ratio.

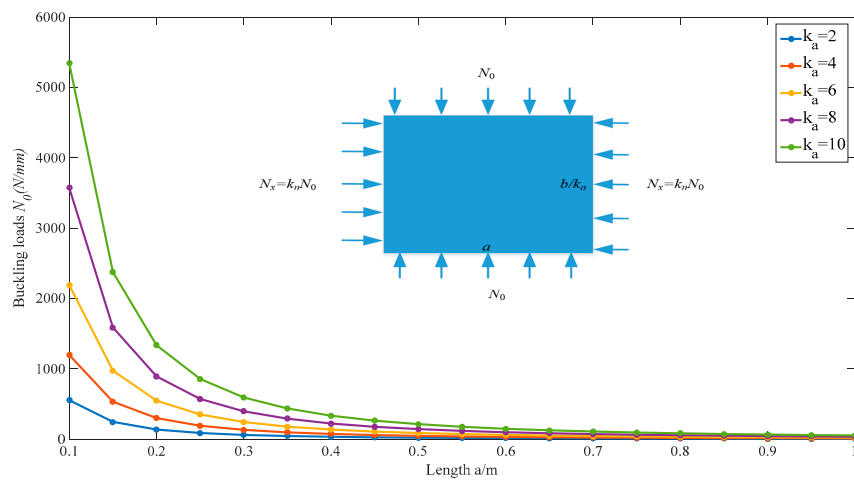


Figure 4. Buckling loads affected by geometrical parameter k_a .

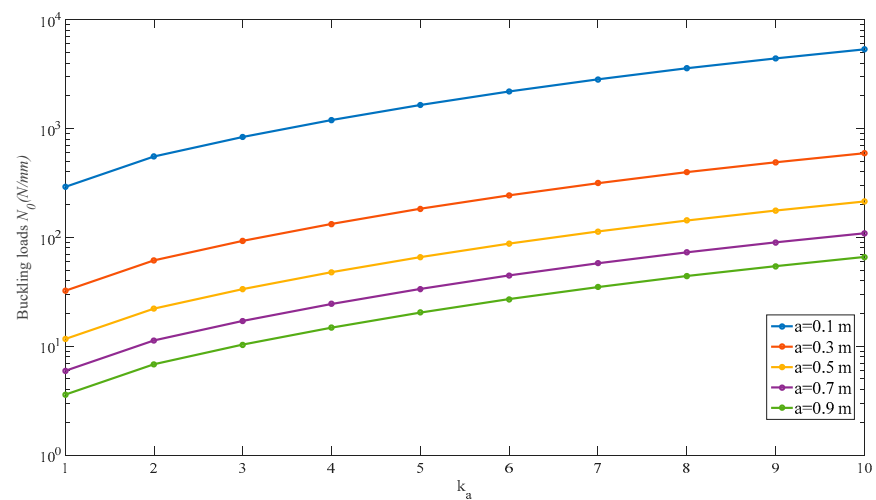


Figure 5. Buckling loads affected by geometrical parameter k_a and the dimensions.

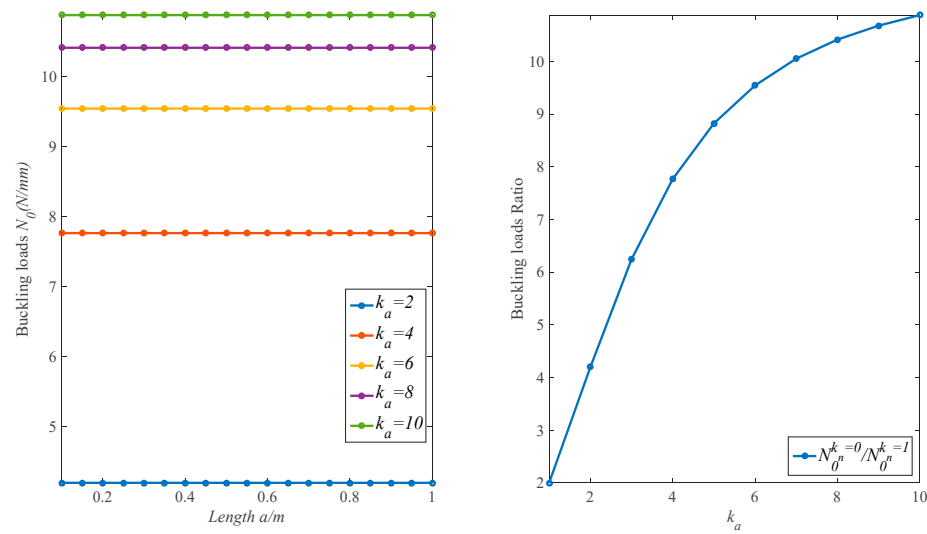


Figure 6. Change rate of buckling loads affected by geometrical parameter k_a and the dimensions.

Table 2. Buckling loads vs. k_a .

a		0.1	0.2	0.3	0.4	0.5	0.6	0.7	0.8	0.9	1
k_a	2	553.83	138.46	61.540	34.61	22.15	15.38	11.30	8.65	6.84	5.54
	4	1198.17	299.54	133.13	74.89	47.93	33.28	24.45	18.72	14.79	11.98
	6	2193.74	548.44	243.75	137.11	87.75	60.94	44.77	34.28	27.08	21.94
	8	3574.88	893.72	397.21	223.43	143.00	99.30	72.96	55.86	44.13	35.75
	10	5346.98	1336.75	594.11	334.19	213.88	148.53	109.12	83.55	66.01	53.47

4.3. Critical Buckling Load Affected by the Load Frequency

The load frequency affects the critical buckling load of the composite structures, which is the same as the results of the analysis performed by Xu et al. [46]. By increasing the loading frequency, the critical buckling loads are regularly increased. Considering the frequency-dependent properties of the viscoelastic material and by analyzing the load frequency influence on the structure’s buckling load, the loading frequency ranging from 1 to 1000 Hz is numerically analyzed in this section. $t_1 = t_3 = 2.5$ mm, $t_2 = 4t_1$, $d_t = 1.5t_1$, $k_n = [-2, -1, 0, 1, 2]$, $a = b = 0.1$ m and $k_a = 1$. As shown in Figure 7, by increasing the loading frequency, the buckling load of the honeycomb reinforced laminated structure is generally increased in the considered frequency, ranging from 1 Hz to 1000 Hz. However, it should be noted that, in the present analysis, the structure’s buckling load, which is influenced by the load’s frequency, can be divided into three sections according to its change rate by red dotted lines, as shown in Figure 7. It is separated into three sections in terms of the load frequency, which are: 1~100.3 Hz, 100.3~700.9 Hz and 700.9~1000 Hz. In the considered frequency ranges, the buckling load of the structure is sharply increased and is then kept stable in a defined range. Then, it goes up significantly, and the critical frequencies are 100.3 Hz and 700.9 Hz. As a key factor that affects the structure’s buckling, the trend of the structure buckling is influenced by the load frequency, which is the same as the normalized effective equivalent stiffness.

4.4. Critical Buckling Load Affected by the Core Layer’s Thickness

The core layer’s thickness of the honeycomb reinforced composite laminated structure directly influences the structure’s dynamic effective equivalent stiffness, and the stiffness further affects the buckling load of the composite structures. In this section, the thickness of the honeycomb reinforcement and viscoelastic material composed layer is analyzed numerically. The geometrical, physical and load parameters are: $t_1 = t_3 = 2.5$ mm, $d_t = 1.5t_1$, $k_n = k_a = 1$ and $a = b$, and the numerical data are provided in Table 3. Similar to that which has been researched, the thickness of the honeycomb and viscoelastic material composed

layer are defined as $t_2 = t_R t_1$. $t_R = \{2, 4, 6, 8, 12, 16\}$. The buckling load of is sharply decreased by increasing the composite laminate’s geometrical dimensions, which is the same as the trend displayed in Figure 8. Moreover, it can be observed from Figures 8 and 9 that the buckling load of the structure is increased by increasing the honeycomb reinforced layer’s thickness. To display the buckling load’s increasing rate on the honeycomb layer’s thickness, Figure 9 is provided. In the figure, the buckling load of the composite honeycomb laminate at $t_R = 2$ is considered as the reference value.

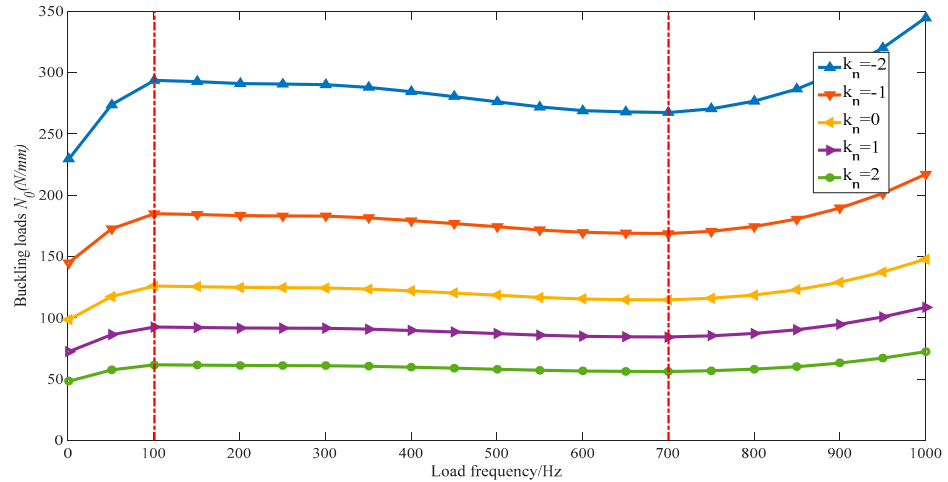


Figure 7. Buckling loads affected by loading frequency.

Table 3. Buckling loads vs. core layer’s thickness.

a	0.1	0.2	0.3	0.4	0.5	0.6	0.7	0.8	0.9	1	
$\frac{t_2}{t_1}$	2	85.38	21.35	9.49	5.34	3.42	2.37	1.74	1.33	1.05	0.85
	4	290.83	72.71	32.31	18.18	11.63	8.08	5.94	4.54	3.59	2.91
	8	1368.22	342.06	152.02	85.51	54.73	38.01	27.92	21.38	16.89	13.68
	12	3785.82	946.45	420.65	236.61	151.43	105.16	77.26	59.15	46.74	37.86
	16	8053.88	2013.47	894.88	503.37	322.16	223.72	164.36	125.84	99.43	80.54

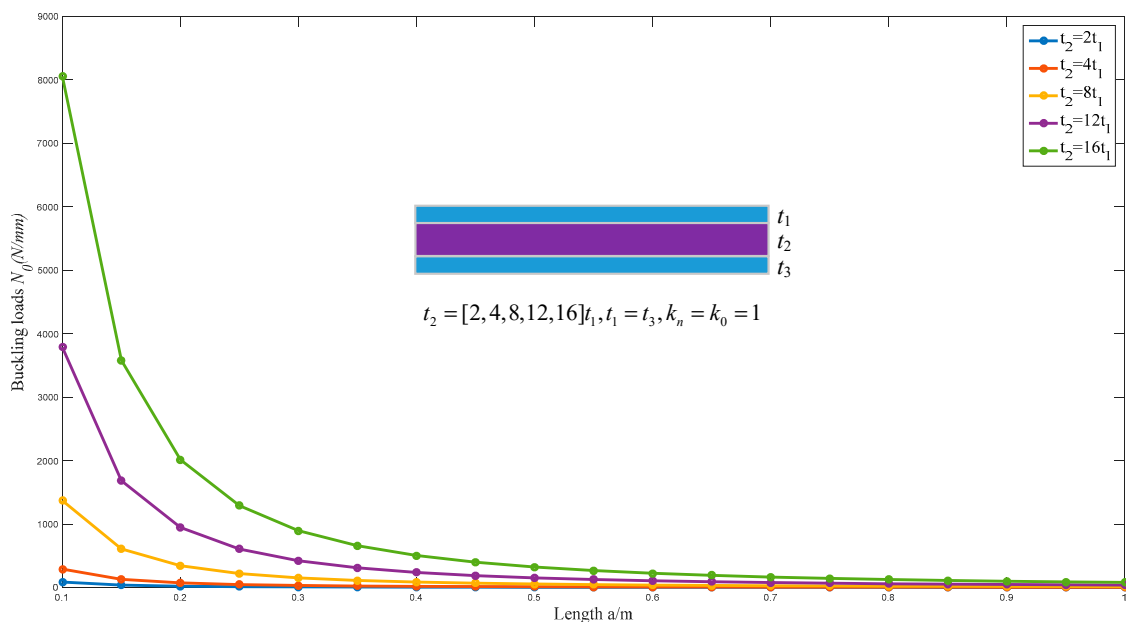


Figure 8. Buckling loads affected by the thickness of the core layer.

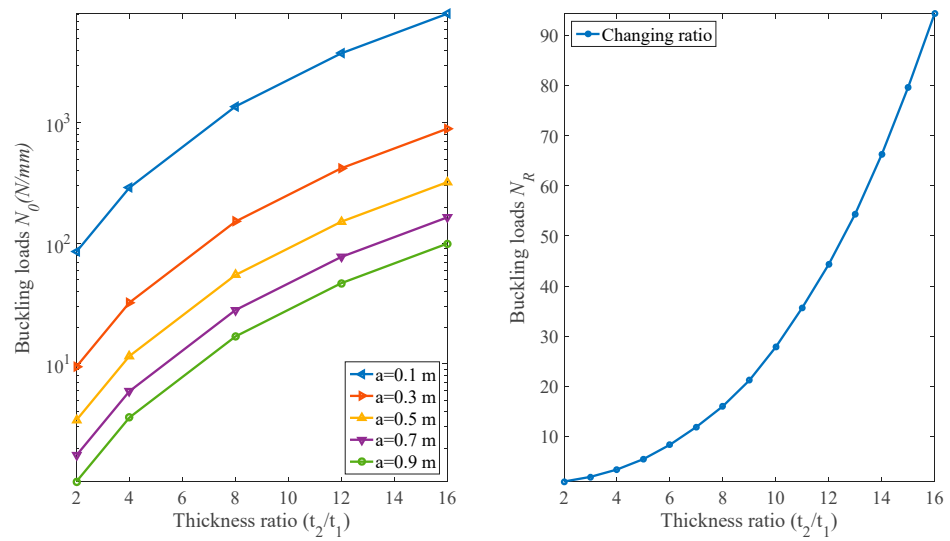


Figure 9. Buckling loads affected by the thickness ratio of the core layer.

4.5. Critical Buckling Load Affected by the Honeycomb Reinforcement's Thickness

The composite structure's dynamic equivalent effective stiffness is directly affected by the honeycomb reinforcement's width. By increasing the reinforcement's width, the dynamic equivalent effective stiffness of the composite structure is increased, and furthermore, the structure's buckling loads in the considered research are significantly influenced. In the present analysis, to illustrate the trend of the buckling load affected by the honeycomb reinforcement's width, a qualitative investigation and quantitative comparison are performed, as plotted in Figures 10 and 11, and the data is showed in Table 4. The physical and geometrical parameters in this section are: $t_1 = t_3 = 2.5$ mm, $t_2 = 5t_1$, $d_t = 1 \sim 4 t_1$, $k_n = k_a = 1$ and $a = b$. It can be seen in Figure 10 that, with the same geometry parameters, the buckling load of the honeycomb reinforced composite laminated structure is sharply increased by raising the reinforcement's width. Moreover, the buckling loads at the defined width of the honeycomb reinforcement are compared in Figure 12. It can be observed that the buckling loads of the composite structure are decreased by increasing the dimensions.

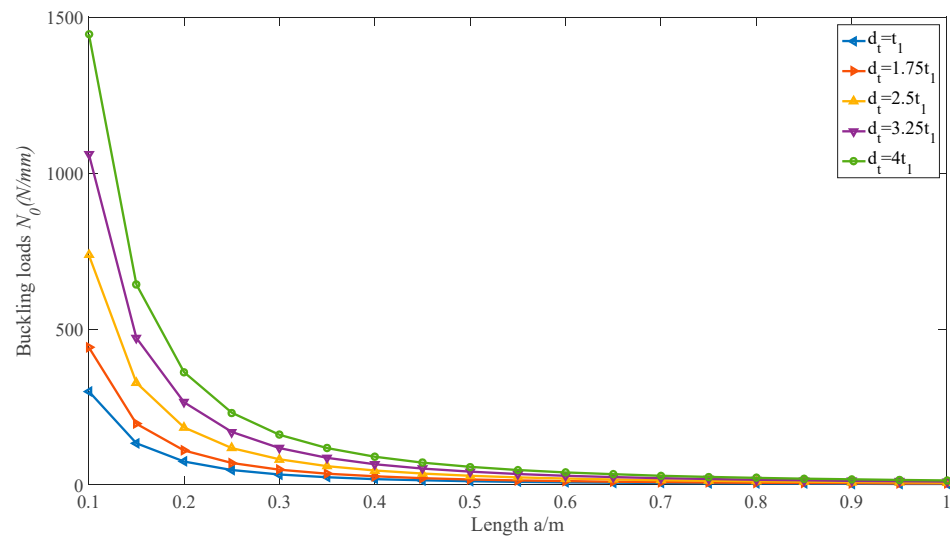


Figure 10. Buckling affected by honeycomb reinforcement's thickness.

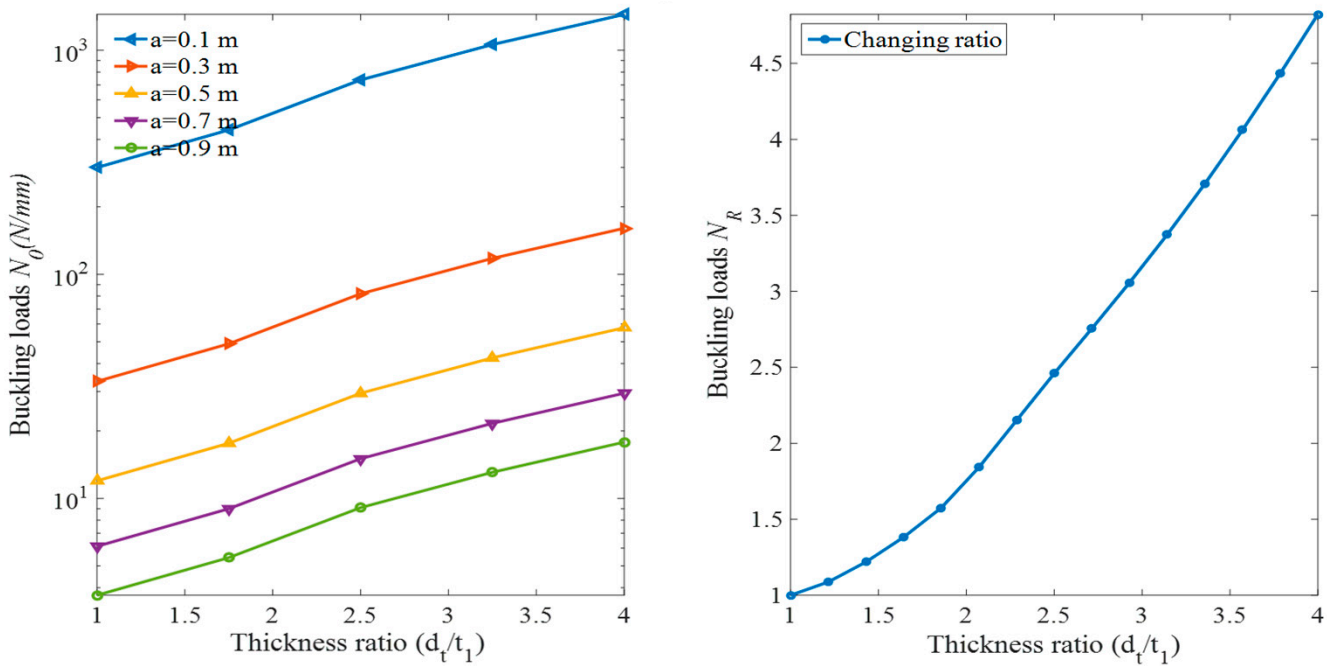


Figure 11. Buckling affected by the thickness ratio of the core layer.

Table 4. Buckling loads vs. wall thickness of honeycomb.

<i>a</i>	0.1	0.2	0.3	0.4	0.5	0.6	0.7	0.8	0.9	1
$d_t/t_1 = 1$	299.73	74.93	33.3	18.73	11.99	8.33	6.12	4.68	3.7	3
$d_t/t_1 = 1.75$	441.04	110.26	49	27.56	17.64	12.25	9	6.89	5.44	4.41
$d_t/t_1 = 2.5$	737.25	184.31	81.92	46.08	29.49	20.48	15.05	11.52	9.1	7.37
$d_t/t_1 = 3.25$	1060.38	265.1	117.82	66.27	42.42	29.46	21.64	16.57	13.09	10.6
$d_t/t_1 = 4$	1445.42	361.36	160.6	90.34	57.82	40.15	29.5	22.58	17.84	14.45

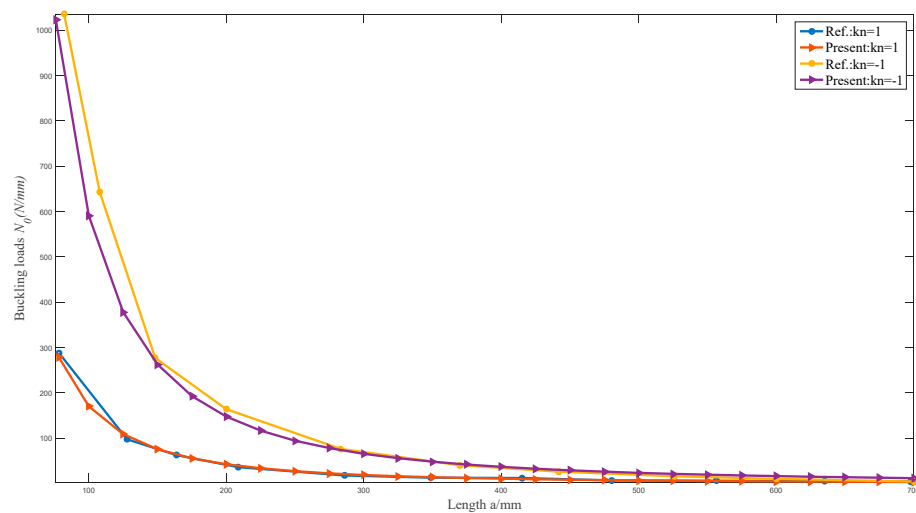


Figure 12. Validation.

5. Validation

In the present analysis, the buckling load of a honeycomb reinforced composite laminated structure is examined by the asymptotic method. To validate the method performed and the results obtained in the present analysis, the structure, which is the same as that which is referred in [37], is established. By submitting the equivalent stiffness of the composite laminate in the method applied in [37], and by defining the load parameter $k_n = 1$ and

$k_n = -1$, the buckling loads obtained by the two methods can be compared. A comparison of the two methods is plotted in Figure 12, and it can be seen that the buckling loads obtained by the asymptotic methods are well consistent with [37]. The calculation error decreases significantly by increasing the structure's geometry dimensions.

6. Conclusions and Discussion

In the present analysis, the buckling load of a honeycomb reinforced laminated structure filled with viscoelastic material is examined by employing the equivalent stiffness parameters obtained through asymptotic methods and the Halpin–Tsai model. The geometrical and physical parameters that influence the composite laminate's buckling loads are qualitatively and quantitatively discussed and compared through an analysis. The following conclusions can be obtained from this research:

- (1) The physical parameters, such as the elastic modulus and shear modulus of the viscoelastic material, are affected by the load's frequencies; accordingly, the buckling loads of the composite structure are influenced by the load's frequency. The trend of the buckling loads affected by the loading frequency is the same as the composite structure's dynamic equivalent effective stiffness, and the original phenomenon can be traced back to the behaviors of viscoelastic materials.
- (2) Buckling loads are affected by the geometry parameters of the composite sandwich structure directly. The buckling load is significantly increased by increasing by the width of the composite structure, but it is decreased sharply by increasing the length of the sandwich structure. This phenomenon shows the same results as those of the buckling analysis of classical beams and plates.
- (3) The composite structure's buckling load is influenced by the honeycomb reinforcement layer's thickness and the honeycomb's width. The main reason is that the equivalent stiffness of the composite sandwich structure is changed by the honeycomb reinforcement's width and height. It should be noted that, by comparing it to the honeycomb reinforcement layer's thickness, the honeycomb's width affects the structure's buckling loads to a relatively smaller degree.

The moisture and temperature of the environment as well as the loading amplitude influence the viscoelastic material's physical parameters as well, which is the same as the frequency-dependent properties. The background temperature in the research is considered to be 20 °C, the loading frequency ranges from 1 to 1000 Hz and the moisture effect on the viscoelastic material is neglected. Moreover, the loading amplitude properties on the viscoelastic material are not taken into consideration. In further research, those factors will be introduced.

Author Contributions: D.Q.: Conceptualization, Investigation, Methodology, Writing—original draft preparation. Q.S.: Methodology, Writing—review and editing. S.Z.: Conceptualization, Methodology, Writing—review and editing. Y.W.: Writing—reviewing and editing, Supervision, Funding acquisition. X.Z.: Writing—reviewing and editing, Methodology, Funding acquisition. All authors have read and agreed to the published version of the manuscript.

Funding: This work was supported by the National Key Research and Development Program of China under Grant No. 2018YFD0700604 and by the Fundamental Research Funds for the Central Universities under Grant No. 2019kfyXJJS192.

Conflicts of Interest: The authors declare that they have no known competing financial interests or personal relationships that could have appeared to influence the work reported in this paper.

References

1. Pearson, C.; Delatte, N. Collapse of the Quebec bridge, 1907. *J. Perform. Constr. Facil.* **2006**, *20*, 84–91. [[CrossRef](#)]
2. Turvey, G.J.; Marshall, I.H. *Buckling and Postbuckling of Composite Plates*; Springer Science & Business Media: Berlin/Heidelberg, Germany, 2012.
3. Wang, C.M.; Wang, C.Y. *Exact Solutions for Buckling of Structural Members*; CRC Press: Boca Raton, FL, USA, 2004.

4. Sayyad, A.S.; Ghugal, Y.M. Bending, buckling and free vibration of laminated composite and sandwich beams: A critical review of literature. *Compos. Struct.* **2017**, *171*, 486–504. [[CrossRef](#)]
5. Namdar, Ö.; Darendeliler, H. Buckling, postbuckling and progressive failure analyses of composite laminated plates under compressive loading. *Compos. Part B Eng.* **2017**, *120*, 143–151. [[CrossRef](#)]
6. Kolahchi, R.; Zarei, M.S.; Hajmohammad, M.H.; Naddaf Oskouei, A. Visco-nonlocal-refined Zigzag theories for dynamic buckling of laminated nanoplates using differential cubature-Bolotin methods. *Thin-Walled Struct.* **2017**, *113*, 162–169. [[CrossRef](#)]
7. Ho-Huu, V.; Do-Thi, T.D.; Dang-Trung, H.; Vo-Duy, T.; Nguyen-Thoi, T. Optimization of laminated composite plates for maximizing buckling load using improved differential evolution and smoothed finite element method. *Compos. Struct.* **2016**, *146*, 132–147. [[CrossRef](#)]
8. Ehsani, A.; Rezaeepazhand, J. Stacking sequence optimization of laminated composite grid plates for maximum buckling load using genetic algorithm. *Int. J. Mech. Sci.* **2016**, *119*, 97–106. [[CrossRef](#)]
9. Huang, L.; Sheikh, A.H.; Ng, C.-T.; Griffith, M.C. An efficient finite element model for buckling analysis of grid stiffened laminated composite plates. *Compos. Struct.* **2015**, *122*, 41–50. [[CrossRef](#)]
10. Chen, Q.; Qiao, P. Buckling analysis of laminated plate structures with elastic edges using a novel semi-analytical finite strip method. *Compos. Struct.* **2016**, *152*, 85–95. [[CrossRef](#)]
11. Arshid, E.; Amir, S.; Loghman, A. Bending and buckling behaviors of heterogeneous temperature-dependent micro annular/circular porous sandwich plates integrated by FGPEM nano-Composite layers. *J. Sandw. Struct. Mater.* **2021**, *23*, 3836–3877. [[CrossRef](#)]
12. Gunawan, D.; Suryoatmono, B. Numerical study on lateral-torsional buckling of honeycomb beam. *Procedia Eng.* **2017**, *171*, 140–146. [[CrossRef](#)]
13. Southward, T.; Mallinson, G.; Jayaraman, K.; Horrigan, D. Buckling of disbonds in honeycomb-core sandwich beams. *J. Sandw. Struct. Mater.* **2008**, *10*, 195–216. [[CrossRef](#)]
14. Li, C.; Shen, H.-S.; Wang, H. Thermal post-buckling of sandwich beams with functionally graded negative Poisson's ratio honeycomb core. *Int. J. Mech. Sci.* **2019**, *152*, 289–297. [[CrossRef](#)]
15. Arefi, M.; Najafitabar, F. Buckling and free vibration analyses of a sandwich beam made of a soft core with FG-GNPs reinforced composite face-sheets using Ritz Method. *Thin-Walled Struct.* **2021**, *158*, 107200. [[CrossRef](#)]
16. Qiu, C.; Guan, Z.; Guo, X.; Li, Z. Buckling of honeycomb structures under out-of-plane loads. *J. Sandw. Struct. Mater.* **2020**, *22*, 797–821. [[CrossRef](#)]
17. Ohno, N.; Okumura, D.; Niikawa, T. Long-wave buckling of elastic square honeycombs subject to in-plane biaxial compression. *Int. J. Mech. Sci.* **2004**, *46*, 1697–1713. [[CrossRef](#)]
18. Miller, W.; Smith, C.W.; Evans, K.E. Honeycomb cores with enhanced buckling strength. *Compos. Struct.* **2011**, *93*, 1072–1077. [[CrossRef](#)]
19. López Jiménez, F.; Triantafyllidis, N. Buckling of rectangular and hexagonal honeycomb under combined axial compression and transverse shear. *Int. J. Solids Struct.* **2013**, *50*, 3934–3946. [[CrossRef](#)]
20. Zhou, X.Q.; Yu, D.Y.; Shao, X.Y.; Wang, S. Asymptotic homogenization analysis of the dynamics properties of periodically and orthogonally stiffened composite laminates. *Compos. Part B Eng.* **2016**, *105*, 116–131. [[CrossRef](#)]
21. Usta, F.; Türkmen, H.S.; Scarpa, F. High-velocity impact resistance of doubly curved sandwich panels with re-entrant honeycomb and foam core. *Int. J. Impact Eng.* **2022**, *165*, 104230. [[CrossRef](#)]
22. Meng, H.; Galland, M.A.; Ichchou, M.; Xin, F.X.; Lu, T.J. On the low frequency acoustic properties of novel multifunctional honeycomb sandwich panels with micro-perforated faceplates. *Appl. Acoust.* **2019**, *152*, 31–40. [[CrossRef](#)]
23. Zhou, X.; Yu, D.; Zhang, S. Homogenous asymptotic analysis on vibration energy dissipation characteristics of periodical honeycomb reinforced composite laminate filled with viscoelastic damping material. *Compos. Struct.* **2021**, *258*, 113307. [[CrossRef](#)]
24. Zhou, X.Q.; Zhang, S.Q.; Lin, W.W. Sound radiation characteristics analysis for the honeycomb reinforced laminated structures with viscoelastic material fillers through the asymptotic homogenous method. *Compos. Struct.* **2020**, *245*, 112266. [[CrossRef](#)]
25. Du, B.; Chen, L.; Wu, W.; Liu, H.; Zhao, Y.; Peng, S.; Guo, Y.; Zhou, H.; Chen, L.; Li, W.; et al. A novel hierarchical thermoplastic composite honeycomb cylindrical structure: Fabrication and axial compressive properties. *Compos. Sci. Technol.* **2018**, *164*, 136–145. [[CrossRef](#)]
26. Eipakchi, H.; Nasrekani, F.M. Vibrational behavior of composite cylindrical shells with auxetic honeycombs core layer subjected to a moving pressure. *Compos. Struct.* **2020**, *254*, 112847. [[CrossRef](#)]
27. Cong, P.H.; Long, P.T.; Van Nhat, N.; Duc, N.D. Geometrically nonlinear dynamic response of eccentrically stiffened circular cylindrical shells with negative poisson's ratio in auxetic honeycombs core layer. *Int. J. Mech. Sci.* **2019**, *152*, 443–453. [[CrossRef](#)]
28. Zhou, X.Q.; Yu, D.Y.; Shao, X.Y.; Zhang, S.Q.; Wang, S. Research and applications of viscoelastic vibration damping materials: A review. *Compos. Struct.* **2016**, *136*, 460–480. [[CrossRef](#)]
29. Zhou, X.Q.; Yu, D.Y.; Shao, X.Y.; Wang, S.; Zhang, S.Q. Asymptotic analysis for composite laminated plate with periodically fillers in viscoelastic damping material core. *Compos. Part B Eng.* **2016**, *96*, 45–62. [[CrossRef](#)]
30. Zhou, X.Q.; Yu, D.Y.; Shao, X.; Zhang, S.Q.; Wang, S. Research on the low frequency band gap properties of periodically composite stiffened thin-plate with fillers. *Thin-Walled Struct.* **2016**, *108*, 41–55. [[CrossRef](#)]
31. Guesmia, A.; Messaoudi, S.A. General energy decay estimates of Timoshenko systems with frictional versus viscoelastic damping. *Math. Methods Appl. Sci.* **2009**, *32*, 2102–2122. [[CrossRef](#)]

32. Saravanan, C.; Ganesan, N.; Ramamurti, V. Vibration and damping analysis of multilayered fluid filled cylindrical shells with constrained viscoelastic damping using modal strain energy method. *Comput. Struct.* **2000**, *75*, 395–417. [[CrossRef](#)]
33. Suhr, J.; Koratkar, N.; Keblinski, P.; Ajayan, P. Viscoelasticity in carbon nanotube composites. *Nat. Mater.* **2005**, *4*, 134. [[CrossRef](#)] [[PubMed](#)]
34. Jung, W.-Y.; Aref, A.J. A combined honeycomb and solid viscoelastic material for structural damping applications. *Mech. Mater.* **2003**, *35*, 831–844. [[CrossRef](#)]
35. Aumjaud, P.; Smith, C.W.; Evans, K.E. A novel viscoelastic damping treatment for honeycomb sandwich structures. *Compos. Struct.* **2015**, *119*, 322–332. [[CrossRef](#)]
36. Gibson, R.F. *Principles of Composite Material Mechanics*; CRC Press: Boca Raton, FL, USA, 2016.
37. Kassapoglou, C. *Design and Analysis of Composite Structures: With Applications to Aerospace Structures*; John Wiley & Sons: Hoboken, NJ, USA, 2013.
38. Timoshenko, S.; Woinowsky-Krieger, S.; Woinowsky-Krieger, S. *Theory of Plates and Shells*; McGraw-Hill: New York, NY, USA, 1959.
39. Reddy, J.N. *Mechanics of Laminated Composite Plates and Shells: Theory and Analysis*; CRC Press: Boca Raton, FL, USA, 2003.
40. Cai, Y.; Xu, L.; Cheng, G. Novel numerical implementation of asymptotic homogenization method for periodic plate structures. *Int. J. Solids Struct.* **2014**, *51*, 284–292. [[CrossRef](#)]
41. Smith, P.A.; Wood, J.R. Poisson's ratio as a damage parameter in the static tensile loading of simple crossply laminates. *Compos. Sci. Technol.* **1990**, *38*, 85–93. [[CrossRef](#)]
42. Halpin, J.C.; Thomas, R.L. Ribbon Reinforcement of Composites. *J. Compos. Mater.* **1968**, *2*, 488–497. [[CrossRef](#)]
43. Halpin, J.C.; Jerine, K.; Whitney, J.M. The Laminate Analogy for 2 and 3 Dimensional Composite Materials. *J. Compos. Mater.* **1971**, *5*, 36–49. [[CrossRef](#)]
44. Afdl, J.; Kardos, J. The Halpin-Tsai equations: A review. *Polym. Eng. Sci.* **1976**, *16*, 344–352. [[CrossRef](#)]
45. Hill, R. Elastic properties of reinforced solids: Some theoretical principles. *J. Mech. Phys. Solids* **1963**, *11*, 357–372. [[CrossRef](#)]
46. Xu, X.; Ma, J.; Lim, C.W.; Chu, H. Dynamic local and global buckling of cylindrical shells under axial impact. *Eng. Struct.* **2009**, *31*, 1132–1140. [[CrossRef](#)]